Phase-resolved HST/STIS spectroscopy of the exposed white dwarf in the high-field polar AR UMa [1]

Boris T. Gänsicke

Universitäts-Sternwarte Göttingen, Geismarlandstr. 11, 37073 Göttingen, Germany

Gary D. Schmidt

Steward Observatory, University of Arizona, Tucson, AZ 85721

Stefan Jordan

Institut für Astronomie und Astrophysik, Universität Kiel, 24098 Kiel, Germany

and

Paula Szkody

Astronomy Department, University of Washington, Seattle, WA 98195

ABSTRACT

[1]Based on observations made with the NASA/ESA Hubble Space Telescope, obtained at the Space Telescope Science Institute, which is operated by the Association of Universities for Research in Astronomy, Inc., under NASA contract NAS 5-26555.

Phase-resolved *HST/STIS* ultraviolet spectroscopy of the high-field polar AR UMa confirms that the white dwarf photospheric Lyα Zeeman features are formed in a magnetic field of ~ 200 MG. In addition to the Lyα π and σ^+ components, we detect the forbidden hydrogen $1s_0 \rightarrow 2s_0$ transition, which becomes "enabled" in the presence of both strong magnetic and electric fields. Overall, the combined ultraviolet and optical low state spectrum is similar to that of the single white dwarf PG 1031+234, in that the optical continuum has a steeper slope than the ultraviolet continuum and that the depth of the Lyα Zeeman lines reaches only $30 - 50\,\%$ of the continuum level. Our attempt in fitting the low state data with single temperature magnetic white dwarf models remains rather unsatisfactory, indicating either a shortcoming in the present models or a new physical process acting in AR UMa. As a result, our estimate of the white dwarf temperature remains somewhat uncertain, $T_{\rm wd} = 20\,000 \pm 5000$ K. We detect a broad emission bump centered at ~ 1445 Å and present throughout the entire binary orbit, and a second bump near ~ 1650 Å, which appears only near the inferior conjunction of the secondary star. These are suggestive of low harmonic cyclotron emission produced by low-level ($\dot{M} \sim 10^{-13}\,M_\odot\,{\rm yr}^{-1}$) accretion onto both magnetic poles. However, there is no evidence in the power spectrum of light variations for accretion in gas blobs. The derived field strengths are $B \sim 240$ MG and $B \gtrsim 160$ MG for the northern and the southern pole, respectively, broadly consistent with the field derived from the Zeeman lines. The observed Lyα emission line shows a strong phase dependence with maximum flux and redshift near orbital phase $\phi \sim 0.3$, strongly indicating an origin on the trailing hemisphere of the secondary star. An additional Lyα absorption feature with similar phasing as the Lyα emission, but a $\sim 700\,{\rm km\,s^{-1}}$ blueshift could tentatively be ascribed to absorption of white dwarf emission in a moderately fast wind. Finally, the high signal-to-noise *STIS* data provide important information on the intergalactic absorption toward AR UMa. We derive a column density of neutral hydrogen of $N_{\rm H} = (1.1 \pm 1.0) \times 10^{18}{\rm cm}^{-2}$, the lowest of any known polar, making AR UMa an excellent candidate for further EUV observations.

Subject headings: stars: individual (AR UMa) – stars: magnetic fields – line: formation – white dwarfs – novae, cataclysmic variables

1. Introduction

AR UMa is a magnetic cataclysmic variable (CV) of the extreme kind. It was discovered as a very luminous soft X-ray source during the *EINSTEIN* slew survey and optically identified as a nearby ($d = 88\,\mathrm{pc}$), short-period ($P_{\mathrm{orb}} = 1.932\,\mathrm{hr}$, near the lower edge of the period gap), and possibly magnetic CV by **?**). An analysis of the Harvard and Sonneberg plate material showed that AR UMa spends most of the time in a state of low accretion activity, $V \sim 16.5$, with sporadic high states reaching up to $V \sim 13.5$ (**??**). **?**) confirmed AR UMa as a strongly magnetic CV (polar) with unprecedented properties: in contrast to all other known polars, AR UMa shows practically *no* circular polarization during the high accretion state. Moderate circular polarization is, however, observed during the low state, and, if interpreted as dichroism in the photosphere of the white dwarf, indicates a magnetic field $B \gtrsim 200\,\mathrm{MG}$. Confirmation of an extremely high field ($B \sim 230\,\mathrm{MG}$) was provided by the detection of the Lyα σ^+ Zeeman component in the *IUE* low state spectrum of AR UMa (**?**). Additional optical (**?**) and EUV/X-ray observations (**?**) constrained the binary parameters and highlighted the central role of the strong magnetic field in the accretion process. Summing up, AR UMa is the first polar than can compete in magnetic field strength with the known single high-field white dwarfs, permitting tests of current theories of magnetically-funneled accretion onto white dwarfs under extreme conditions. Two additional systems were recently identified to bridge the magnetic field strength distribution down to the bulk of the polars; V884 Her with $B \approx 150\,\mathrm{MG}$ (**?**) and RX J1007.5−2016 with $B \approx 90\,\mathrm{MG}$ (**?**).

We report in this paper the results of high-quality *HST/STIS* observations of AR UMa which were aimed at an analysis of the properties of the accreting white dwarf. The new data clearly confirm a field strength of $\sim 200\,\mathrm{MG}$, though a detailed modeling of the spectra fails for yet unknown reasons. The *STIS* spectra of AR UMa show some evidence for low-level accretion activity during the low state and such a low interstellar absorption column that the object is an ideal target for future EUV observations.

2. *HST/STIS* observations

STIS observations of AR UMa were carried out on 1998 December 9 during five consecutive *HST* orbits. The optical monitoring of AR UMa reported by **?**) shows that the *HST* data were obtained during a low state ($V \sim 16.5$). The last active phase of AR UMa prior to the *HST* observations was detected in October/November 1998 at an intermediate magnitude of $V \sim 15.5$. Considering that AR UMa was faint in June 1998, this active state might have lasted for a maximum of ~ 5 months. Unfortunately, during July–September, AR UMa is too close to the sun, preventing continuous monitoring. The bulk of the *STIS* data were

obtained with the G140L far-ultraviolet (FUV, 1130−1710 Å) grating; only a single short G230L near-ultraviolet (NUV, 1660−3150 Å) exposure was obtained during the last orbit of the visit (Table 1). All data were taken through the $52'' \times 0.2''$ slit in order to optimize both throughput and spectral resolution ($R \approx 1000$ and $R \approx 500$ for the G140L and the G230L data, respectively).

2.1. The average *STIS* spectrum

The strongest features detected in the average *STIS* spectrum of AR UMa (Fig. 1) are the broad absorption troughs of the Lyα π and σ^+ Zeeman components. This confirms the identification of the absorption line observed at ~ 1300 Å in the *IUE* low state spectrum as Lyα σ^+ split in a field of ~ 230 MG (**?**). At such field strengths, the σ^- component falls shortwards of the wavelength range covered by *STIS*, and the strong decrease in flux observed below 1145 Å is due to the rapid drop of the *STIS* sensitivity toward shortest wavelengths.

The high-quality *STIS* data (signal-to-noise ratio ~ 30 at $1150\,\text{Å} < \lambda < 1450\,\text{Å}$ and ~ 20 at $1450\,\text{Å} < \lambda < 1750\,\text{Å}$ in the average FUV spectrum) reveals two additional absorption-like structures centered at 1180 Å and 1415 Å, as well as a number of weak, narrow absorption lines which are most likely of interstellar origin (Fig. 1). Note that the average spectrum contains *two* narrow Lyα absorption lines, centered at velocities zero and $\sim -700\,\text{km s}^{-1}$. Finally, the weakness of the detected emission lines, Lyα, C IV λ1550, and Mg II λ2800, confirms that AR UMa was in a state of very low accretion activity at the time of the *HST* observations.

2.2. Phase-resolved ultraviolet spectroscopy

The G140L data were obtained over 1.7 binary orbits with strong phase overlap between the five exposures. We used the `inttag` and `calstis` commands of STSDAS to split the G140L datasets (Table 1) into 4, 5, 5, 5, and 3 subexposures, respectively, with individual exposure times ranging from 440 s to 592.5 s (corresponding to orbital phase resolutions $\Delta\phi \approx 0.06 - 0.09$). The phases of mid-exposure of the 22 spectra were computed using the ephemeris of **?**), where $\phi = 0$ corresponds to the inferior conjunction of the secondary star. Finally, the sub-exposures were summed up in five phase bins to increase the signal-to-noise ratio (Figure 2). The spectral features that noticeably change around the orbit are (1) the 1180 Å absorption, being strongest at $\phi \approx 0.5$, (2) the Lyα emission, being strongest at

$\phi \approx 0.3$ and absent shortly before the inferior conjunction of the secondary star at $\phi \simeq 0.9$, and (3) a very broad ($\sim$ 200 Å) and weak emission centered at $\sim$ 1650 Å that appears between $\phi \simeq 0.9 - 1.1$

3. The photospheric white dwarf spectrum

During a low state, the ultraviolet/optical emission of a polar is dominated by the photospheric spectra of the white dwarf and of the secondary star, allowing a direct measurement of quantities such as the magnetic field strength and the effective temperature of the white dwarf and the spectral type of the secondary (**?**, e.g.)]schmidtetal81-1,schwopeetal93-1. In AR UMa, **?**) clearly showed that the red end of the optical spectrum reveals the emission of an M6 dwarf, and derived a distance of 88 pc. For the present analysis, we supplement our *HST/STIS* spectra with an optical low-state spectrum obtained on 1998 May 22 with the CCD Spectropolarimeter (**?**) and 2.3 m Bok telescope on Kitt Peak. The latter data cover the region 4000-8000 A at a resolution of $\sim$ 12 Å, and result from a 300 s exposure ($\Delta\phi \sim 0.04$) centered at $\phi = 0.79$. The use of these non-simultaneous data is justified by the fact that the low-state brightness of AR UMa has historically shown very little evidence for change once the system cools from an active phase (**???**), and because the continuum ($V = 16.9$) in the May 1998 data is within 0.1 mag of a V-band measurement obtained 1998 Nov 14, just 3 weeks prior to the *HST* observations.

3.1. White dwarf temperature

?) fitted the combined *IUE*/optical low state spectrum of AR UMa using a grid of solar abundance non-magnetic white dwarf model spectra from **?**). They found that no satisfying fit can be achieved with a single-temperature model, but that a 15 000 K white dwarf with a 35 000 K spot covering 2 % of the white dwarf surface provides a rough match for the data. It is clear that any analysis based on non-magnetic models is necessarily prone to large uncertainties, as the strong magnetic field has a major impact on the bound-free and bound-bound opacities in the white dwarf atmosphere (**?**, e.g.)]meranietal95-1.

Figure 3 illustrates the discrepancy between the observed overall spectrum of AR UMa and non-magnetic pure hydrogen white dwarf model spectra. The optical spectrum of AR UMa is very blue, almost Rayleigh-Jeans, and can be described well with a 50 000 K

non-magnetic white dwarf model spectrum[2]. In contrast to this, the *STIS* FUV/NUV spectrum is relatively flat, suggesting $T_{\rm wd} \sim 15\,000$ K. If we assume a distance of 88 pc (**?**), fitting the flux of the ultraviolet data with the 15 000 K model yields a white dwarf radius of $R_{\rm wd} = 10^9$ cm, which corresponds to emission from the entire white dwarf. In contrast, the 50 000 K fit to the optical data can only be interpreted as emission from a small spot on the white dwarf. This mismatch of the ultraviolet and the optical continuum is actually *the opposite* of what is expected from a white dwarf plus hot spot model. In such a configuration, the ultraviolet range is dominated by the hot spot and has a steeper slope than the optical range which reveals the cooler underlying white dwarf (**?**, e.g.)]gaensickeetal00-1.

Very similar problems were encountered by **?**) when interpreting the ultraviolet and optical spectrum of the *single* magnetic white dwarf PG 1031+234 ($B \sim 500$ MG). Also in this star, which certainly has no accretion-heated pole cap, the ultraviolet continuum is relatively flat, corresponding to $T_{\rm wd} \approx 15\,000$ K, while the optical continuum is steeper, indicating $T_{\rm wd} \approx 25\,000$ K.

We attempted a better description of the observed ultraviolet plus optical low state spectrum of AR UMa using the magnetic white dwarf model spectra of **?**) (**?**, see also)]putney+jordan95-1,burleighetal99-1, assuming a magnetic field of $B = 200$ MG (**?**). We computed the spectra for an angle of 20° between the line-of-sight and the magnetic axis, which corresponds to the closest approach of the magnetic pole to the observer (**?**). The positions of the Lyα components are well reproduced, confirming the field strength derived by **?**). Figure 3 shows the low state data of AR UMa along with magnetic white dwarf model spectra for $T_{\rm wd} = 15\,000$, 20 000, and 25 000 K. The mismatch between the optical and the ultraviolet continuum is somewhat alleviated compared to the fit with non-magnetic models, but, again, no single-temperature model provides a satisfactory fit to the overall spectrum of AR UMa. The scaling applied to the magnetic model spectra in Fig. 3 implies white dwarf radii of 5.1×10^8 cm and 4.3×10^8 cm for the 20 000 K and the 25 000 K models, respectively, for a distance of 88 pc (**?**). These values are compatible with the assumption that the low state spectrum of AR UMa is dominated by emission from the magnetic white dwarf.

We also attempted to model the *STIS* FUV data alone with our magnetic white dwarf spectra, again with only limited success: Fig. 4 shows the best match with $T_{\rm wd} = 17\,000$ K and $R_{\rm wd} = 8.2 \times 10^8$ cm (for $d = 88$ pc). While the FUV continuum is well described, the model over-predicts the optical flux in the V band by a factor of ~ 2. Interestingly, the Zeeman lines of the model spectra are more deeply modulated and have, hence, larger equivalent widths

[2]The extremely steep low-state spectrum of AR UMa was already noted by **?**) who compared it in their Fig. 1 with the low-state spectrum of AM Her, which has $T_{\rm wd} \approx 20\,000$ K (**??**).

than the observed lines. Again, this is very similar to the observations of PG 1031+234, where the Lyα σ^+ component is modulated only to $\sim$50 % of the continuum flux. **?**) argued that the Zeeman transitions can only absorb one of two orthogonal polarization modes of the outgoing flux and, hence, the depth of a saturated line will reach maximally 50 % of the continuum level.

A quantitative prediction of the line depth and strength is complicated, as magneto-optical effects (Faraday rotation and Voigt effect) change the polarization properties of the absorption coefficients throughout the atmosphere. In addition, there is at present no reliable theory for the Stark broadening of the individual Zeeman components in the presence of a strong magnetic field. We carried out two exploratory model atmosphere calculations for $T_{\rm wd} = 20\,000$ K, $B = 200$ MG, once including and once excluding the magneto-optical effects. The strongest transition, the Lyα π component, is modulated to ~ 50 % in the spectrum that was computed without magneto-optical effects, just as expected according to **?**). However, the π component is almost 100 % modulated in the spectrum that was computed including the magneto-optical effects. Similar variations are observed in the σ^+ and σ^- components. We have, thus, to conclude that at present it is not possible to self-consistently model the spectrum of the magnetic white dwarf in AR UMa (or that of PG 1031+234).

Just for completeness, we note that AR UMa as an interacting binary offers two other possibilities to explain the low depth of the Lyα lines: either another component in the binary contributes significantly to the FUV flux, or the white dwarf atmosphere is heated by accretion, resulting in a flatter vertical temperature gradient and weaker absorption lines (as observed e.g. in AM Her during a high state; **?**). However, neither hypothesis is very appealing, as AR UMa was observed with *HST* during a state of very low accretion activity.

3.2. The 1180 Å absorption line: a forbidden Lyα $\mathbf{1s_0 \rightarrow 2s_0}$ component in the atmosphere of the white dwarf?

In addition to the Lyα π and σ^+ components, a relatively broad (FWHM$\sim$11Å) absorption feature centered at ≈ 1180 Å appears during $\phi = 0.3 - 0.7$ without noticeable variation in wavelength (Fig. 2). Comparison with the phase-resolved *HST/GHRS* spectra of the single magnetic white dwarf RE J0317–853 suggests that the 1180 Å absorption is due to the normally forbidden dipole transition of hydrogen $1s_0 \rightarrow 2s_0$, which becomes increasingly more probable in the presence of both strong magnetic and electric fields, a situation encountered in the high-density atmospheres of magnetic white dwarfs (**?**). In RE J0317–853, the $1s_0 \rightarrow 2s_0$ absorption is attributed to the weaker pole with $B \sim 200$ MG. In AR UMa, the 1180 Å is strongest at $\phi = 0.3 - 0.5$ when the northern magnetic pole $B \sim 240$ is best

visible (see Sect. 3.3.3).

Both the wavelength and the oscillator strength of the $1s_0 \rightarrow 2s_0$ component depend on the choice of the electric field. The oscillator strength of this "forbidden" feature increases with the electric field at the expense of the normal π ($1s_0 \rightarrow 2p_0$) component. Since we have at present the necessary atomic data only for a limited range of electric field strengths we assumed in our model spectrum calculation (Fig. 4) the same electric field of 10^8 V/m as for RE 0317–853 (**?**). A detailed modeling of the $1s_0 \rightarrow 2s_0$ feature, especially of its phase-dependence, will be possible only once the necessary atomic data for a large range of fields are available.

The observed $1s_0 \rightarrow 2s_0$ in AR UMa is stronger than in the model, in fact of similar strength as the observed π ($1s_0 \rightarrow 2p_0$) component! Therefore, the electric field in the atmosphere of AR UMa should be even higher than in that of RE0317–853, which could also explain the slight difference in wavelength between model and observation. Unfortunately, we have no good physical explanation for the origin of such a strong electric field in the atmosphere of AR UMa: The strength of the electric micro field expected from the disturbing particles, ions and electrons, scales with the electron density as $N_e^{2/3}$, which implies that the electric field increases with the effective temperature because of a higher degree of ionization. From this simple assumption, the electric field strength in AR UMa should be a factor of ~ 3 *lower* than in RE 0317–853. A similar conclusion holds for the thermally induced motional Stark effect or the generation of electric fields from a rotating dynamo.

Finally, we add as a cautionary remark that, as the white dwarf in AR UMa is accreting metal-rich material from its secondary, we cannot rule out that heavy elements could contribute to the observed line spectrum. **?**) already argued that a number of absorption lines in the optical spectrum could be from elements other then hydrogen. In fact, a broad (FWHM$\sim$8 Å) absorption is observed in the *STIS* spectrum at ~ 1335 Å, as well as a few narrow features that cannot be explained with interstellar absorption (see Sect. 4), e.g. 1227.7 Å and 1325.6 Å. We note that the 1180/1335 Å features coincide with C III λ 1176 and C II λ 1335, which are very strong in $\sim 20\,000 - 30\,000$ K metal-rich atmospheres. However, in the absence of theoretical descriptions of metal transitions in strong magnetic fields and as no other typically strong absorption, e.g. near Si II λ 1260,65 or Si III λ 1300, is observed, we consider the hydrogen $1s_0 \rightarrow 2s_0$ transition to be the most likely explanation of the 1180 Å feature.

3.3. The broad 1415 Å absorption

The average spectrum (Fig. 1) contains a strong and broad (~ 70 Å) absorption-like feature centered at ~ 1415 Å. From Fig. 2 it appears that this absorption does not significantly depend on the orbital phase. We envision several possible mechanisms that could be the source of this feature.

3.3.1. Quasi-molecular H_2^+ absorption.

In non-magnetic DA white dwarfs with effective temperatures below $\sim 20\,000$ K, absorption by quasi-molecular hydrogen causes a broad line centered at ~ 1400 Å (**?**). **?**) fitted the combined *IUE*/optical low state spectrum of AR UMa with a 15 000 K white dwarf with a small 35 000 K spot (see also the discussion in Sect. 3.1). Such a low temperature of the white dwarf makes the H_2^+ hypothesis appear viable. However, present theory can not predict the position/shape of the H_2^+ absorption in a strong magnetic field. Also on observational grounds, the evidence for H_2^+ absorption in magnetic white dwarfs is meagre: **?**) detected H_2^+ absorption in only two out of 12 *single* magnetic white dwarfs that were observed with *IUE*, and in none of the accreting magnetic white dwarfs in polars observed so far in the ultraviolet.

3.3.2. Zeeman absorption by Balmer lines

In extremely strong magnetic fields several transitions of the Balmer line series are shifted by up to thousands of Å into the ultraviolet (**?**, e.g.)]henry+oconnell85-1. It may, hence, be also possible that the observed absorption near 1415 Å, the phase-dependent flux variation around 1650 Å, and other structures in the long-wavelength portion of the *STIS* spectrum, are related to Balmer absorption. Indeed, our model spectra (Fig. 3) qualitatively reproduce the undulations observed in the NUV spectrum of AR UMa, however they do not contain significant structure in the FUV range (apart from Lyα).

3.3.3. Cyclotron emission – ongoing accretion

Another possible interpretation arises if the structure near 1415 Å is not due to absorption, but if there is a rather broad *emission* bump redward of it, peaking at ~ 1445 Å. In the context of accreting magnetic white dwarfs, cyclotron emission is an immediate can-

didate for the origin of such a broad emission line. As the shape of the feature does not change significantly around the orbit we would have to assume that it originates in a hot accretion plasma near the northern magnetic pole, which remains constantly in view (**??**). The cyclotron hypothesis finds some support in the fact that an additional bump centered at $\sim 1650\,\text{Å}$ appears in the FUV spectrum near $\phi \approx 0$. The spectral shape of this bump is most clearly seen in the flux difference $(\phi = 0.5) - (\phi = 0.0)$, see Fig. 5, right panel, bottom curve. The appearance of the 1650 Å bump coincides with the phase when the southern accretion region rotates into view (**??**), and might be related to accretion onto the southern magnetic pole. We recall here that the southern pole is the more active one during the high state.

We model the hypothetical cyclotron features with the emission of an isothermal plasma slab in a strong magnetic field. The intensity spectrum is simply given as $I_\lambda = B_\lambda(1 - e^{-\tau_\lambda})$, with B_λ the Planck function and τ_λ the wavelength-dependent optical depth. We follow the general approach (**?**, see e.g.)]wickramasinghe88-1 and express $\tau_\lambda = \Lambda\varphi_\lambda$ with the Λ the dimensionless size parameter and φ_λ the dimensionless absorption coefficient (**?**, computed according to)]chanmugam+dulk81-1,thompson+cawthorne87-1. Free parameters of this model are the angle ϑ between the line of sight and the magnetic field line threading the emitting plasma, the magnetic field strength B, the plasma temperature kT, and the size parameter Λ. The detection of a single cyclotron harmonic does not allow an independent estimate of the magnetic field strength. We computed, therefore, the cyclotron model spectra for a range of field strengths that are compatible with $B \simeq 200\,\text{MG}$, as derived from the Zeeman-split Lyα line (Sect. 3.1).

In a first step, we modeled the 1445 Å emission bump in the FUV spectrum obtained at $\phi = 0.5$, as it is least contaminated by the emission bump at 1650 Å. We obtain a satisfactory fit for $B = 240\,\text{MG}$, $kT = 0.45\,\text{keV}$, $\vartheta = 35°$, and $\log(\Lambda) = 7.0$ (bottom curve of Fig. 5, left panel). For these parameters, the 1445 Å bump corresponds to the third harmonic of the cyclotron emission. The model spectrum predicts some emission in the second harmonic at $\sim 2230\,\text{Å}$, and very little flux (a few $10^{-17}\text{erg cm}^{-2}\text{s}^{-1}\text{Å}^{-1}$) in the fundamental frequency at $\sim 4470\,\text{Å}$. The NUV spectrum shows a small change in slope at $\sim 2100\,\text{Å}$, which might be related to flux from the second harmonic. Subtracting the cyclotron model from the observed FUV spectrum results in an almost smooth continuum (Fig. 5, left panel). The remaining structure is not too surprising, as the accretion region will be characterized by a temperature and density structure which can not fully be described by our simple model.

Subsequently, we modeled the 1650 Å emission bump which appears at $\phi \approx 0.0$ with a second cyclotron spectrum for $B = 160\,\text{MG}$, $kT = 0.45\,\text{keV}$, $\vartheta = 35°$, and $\log(\Lambda) = 9.9$ (Fig. 5, bottom panel). This time, the FUV cyclotron bump corresponds to the fourth

harmonic. Some emission is predicted in the third ($\sim$ 2230 Å) and second ($\sim$ 3350 Å) harmonics, and practically no power is expected in the fundamental frequency ($\sim$ 6700 Å).

For both emission regions, the derived model parameters imply an emitting area $A_{\rm cyc} \sim 10^{14}{\rm cm}^2$ and a luminosity $L_{\rm cyc} \sim 10^{30}{\rm erg\,s}^{-1}$. For a canonical white dwarf mass and radius ($0.6\,M_\odot$, $8.4 \times 10^8\,{\rm cm}$), the cyclotron luminosity corresponds to an accretion rate of $\sim 10^{13}{\rm g\,s}^{-1}$, or $\sim 1.7 \times 10^{-13}\,M_\odot\,{\rm yr}^{-1}$.

In summary, if the 1445 Å/1650 Å bumps are really due to cyclotron emission, the implication is that a very low inflow of material feeds both the northern and the southern pole during the low state. The low cyclotron flux that both poles emit in the fundamental harmonics is consistent with the non-detection of low-state cyclotron emission (both in polarization and in flux) in the optical range (**?**). The derived cyclotron luminosity is somewhat larger than the limit on the low state hard X-ray luminosity obtained from ASCA data (**?**). The plasma temperature that we derive is extremely low, but compatible with the combination of a low accretion rate and the efficient cyclotron cooling of the post shock flow in a strong field (**?**, e.g.)]beuermann+woelk96-1. **?**) present updated model temperature structures for accretion columns in polars and predict indeed low-temperature ($kT \lesssim 1\,{\rm keV}$) bremsstrahlung from the accretion region for such a combination.

The field strengths derived from the cyclotron emission may be considered an indication that the field geometry is not that of a simple dipole. Such conclusions are not unusual in the studies of single and accreting magnetic white dwarfs (**?**, e.g.)]wickramasinghe+martin79-1,burleighetal99-1,schwopeetal93-1. However, the derived 160 MG should be considered as a lower limit on the field strength of the southern pole, as the magnetic south pole remains eclipsed by the white dwarf throughout the entire binary orbit (**?**). The detection of cyclotron radiation from the southern accretion region implies that this region is rather extended – which is not too surprising: because of the high magnetic field strength in AR UMa material is already magnetically threaded near the secondary star and may, consequently, be distributed over large areas near the magnetic poles of the white dwarf. The observed weak orbital dependence of the 1445 Å bump requires that the northern cyclotron emitting region must be located very close ($5^\circ - 10^\circ$) to the rotation axis of the white dwarf to minimize the orbital variation of ϑ. **?**) derived from a number of observational constraints a colatitude of the magnetic pole $10^\circ \lesssim \delta_{\rm B} \lesssim 35^\circ$. Keeping in mind that the actual accretion region(s) in polars are usually offset by some degree from the magnetic pole(s), these conclusions are consistent.

4. Narrow absorption lines of low ionization species: ISM

Besides the broad Lyα Zeeman components, the mean spectrum of AR UMa displays a number of narrow absorption lines of various strengths. An enlargement of the FUV average spectrum (Fig. 1) shows that some of the more pronounced narrow absorption features coincide with the strongest interstellar absorption lines that are expected in the spectrum of a nearby galactic ultraviolet-bright source (**?**, e.g.)]gaensickeetal98-2,holbergetal99-1,maucheetal88-1. The most convincing detections are Lyα, Si II λ 1260.4, and C II λ 1334.5 (the latter being embedded in a much broader – FWHM$\sim$8 Å – absorption trough that can not be of interstellar origin, see Sect. 3.2). The interstellar origin of these narrow features is supported by the fact that only the blue component of the Si II $\lambda\lambda$ 1260.4, 1264.7 doublet is present in the spectrum of AR UMa. The red component corresponds to a transition from an excited level which is not populated in the interstellar medium. The interstellar lines of Si II λ 1260.4 and C II λ 1334.5 have equivalent widths of $30 - 50$ mÅ, about half of what is observed in AM Her (**?**). For completeness, we show in Fig. 1 the positions of other interstellar transitions of somewhat lower strength than the observed Si II and C II lines, i.e. Si II $\lambda\lambda$ 1190.70,1193.29, N I λ 1200, O I λ 1302.2, and Si II λ 1304.4. We can not claim a significant detection of any of these lines, but we note that all transitions coincide with absorption dips at the noise level.

The observed interstellar Lyα absorption can be used to derive an estimate of the column density of neutral hydrogen along the line of sight to AR UMa. We use for this purpose the FUV spectrum obtained shortly before inferior conjunction of the secondary ($\phi = 0.9$), where the interstellar Lyα profile is least contaminated by the phase-dependent Lyα emission (Fig. 2). We fitted a pure damping profile (**?**) folded with a 1.2 Å FWHM Gaussian to the observed Lyα absorption line (Fig. 6, top panel). The resulting column density of *neutral* hydrogen is $N_{\rm H} = (1.1 \pm 1.0) \times 10^{18}{\rm cm}^{-2}$. This value is even lower than that derived by **?**) from EUVE observations, $N_{\rm H} = (6 - 10) \times 10^{18}\,{\rm cm}^{-2}$. The higher column density determined from X-ray data indicates the presence of material along the line of sight, presumably within the binary system, in which hydrogen is ionized to a high degree while the other elements are only partially ionized and still contribute to the soft X-ray absorption. We note in passing that AR UMa is the polar with the *lowest* column density identified so far. As it is also a very bright EUV source, it is *the* candidate for future EUV/soft X-ray observations, e.g. searching for spectroscopic evidence of metals in the footpoint of the accretion column.

5. Evidence for a wind in AR UMa?

The FUV spectrum of AR UMa (Fig. 1) displays phase-dependent Lyα emission, as well as a weak absorption centered at ~ 1213 Å (in addition to the interstellar Lyα absorption). Figure 6, bottom panel, shows the Lyα region of the FUV spectra, corrected for an interstellar absorption of $N_{\rm H} = 1.1 \times 10^{18}{\rm cm}^{-2}$.

We fitted the Lyα emission in all 22 short subexposures (Sect. 2.2) with Gaussians in order to derive the variation of the flux and the velocity of the line (Fig. 7). The parameters derived for the spectra covering $\phi = 0.5 - 1.0$ are very uncertain, as the Lyα emission almost vanishes during these phases. A sine fit to the emission line velocities results in a half-amplitude $K = \sim 367 \pm 58\,{\rm km\,s^{-1}}$, a mean velocity $\gamma = 222 \pm 43\,{\rm km\,s^{-1}}$, and maximum redshift occurring at $\phi = 0.31 \pm 0.03$. These parameters are, apart from the higher γ velocity in the ultraviolet data, very similar to those derived from the radial velocities of Hα and Hβ observed in the low state. Every case of strong Lyα emission occurs with a significant redshift, suggesting that the emitting region is moving away from us at $\phi \approx 0.3$. The only component in the binary which is doing this at the given orbital phase is the secondary star (a weak stream would still be expected to show a blueshift or no net velocity near this phase). It seems, therefore, plausible to identify the secondary star as the origin of the Lyα emission. The width of the Lyα emission (FWHM $\approx 570\,{\rm km\,s^{-1}}$) is, however, significantly larger than the rotational broadening on the tidally locked secondary star, indicating that the emission region is not stationary on or near the surface of the secondary.

The phase of maximum Lyα flux is $\phi \approx 0.3$, which corresponds to the best view onto the trailing hemisphere of the irradiated secondary star. The EUVE spectrum of AR UMa shows strong He II λ304 emission at $\phi \approx 0.4$, indicating that the secondary star is, at least during the high state, not irradiated uniformly, i.e. the leading hemisphere is probably shielded by the accretion stream (**?**). The Lyα emission appears to become increasingly double peaked between $\phi \approx 0.3 - 0.5$, with the "dip" in the line core centered at 1216.5 Å. This could indicate either additional absorbing neutral hydrogen in the line of sight with a velocity of $\sim 250\,{\rm km\,s^{-1}}$, or that the Ly$\alpha$ emission consists of two components, which would also be an explanation for the relatively large width of the Lyα emission (see above).

The absorption component at ~ 1213 Å is also strongest at $\phi \approx 0.3$, favoring a common origin of both, the emission and the absorption feature. Identifying the absorption with Lyα yields a velocity of $\sim -700\,{\rm km\,s^{-1}}$. The width of the absorption feature is, in contrast to the Lyα emission, relatively narrow and indicates a low velocity gradient in the absorbing material. In addition, the wavelength of the absorption component does not vary significantly with the orbital phase. The general shape of the Lyα absorption/emission compound is reminiscent of a P Cygni profile, and, hence, very suggestive of the existence of a moderately

fast wind. In a somewhat speculative way, we attribute this Lyα feature to a wind originating from the asymmetrically irradiated secondary star. The narrow, almost stationary absorption corresponds in this case *not* to the absorption of light from wind source – the secondary star (as it does not contribute at all to the ultraviolet flux), but could be related to absorption of light from the white dwarf by the intervening wind material.

One may be prone to suggest the accretion stream as an alternative origin of the Lyα absorption/emission compound. This possibility seems, however, rather unlikely: around $\phi \approx 0.3$, only the footpoint of the accretion stream feeding the northern pole could absorb light from the white dwarf surface, but has at this point a *receding* velocity of several $1000\,\mathrm{km\,s^{-1}}$.

6. Ultraviolet light curves

All the *STIS* data (Table 1) were obtained using the MAMA detectors in the time-tagged mode. The prime data product of the detectors are photon event tables which list the arrival time t and the detector coordinates (x, y) for each registered photon. The time resolution of the MAMA's is $125\mu\,\mathrm{s}$. This data format permits the extraction of light curves in arbitrary wavelength bands and with any desired time resolution.

6.1. Orbital flux modulation

We chose to produce light curves from the G140L observations in the four wavelengths listed in Table 2. The bands were selected to avoid the geocoronal Lyα emission[3] and to provide roughly even sampling over the observed FUV range.

The first step in extracting the light curves is to select appropriate (x, y) regions in the raw two-dimensional detector image which contain the desired wavelength range of the object spectrum, as well as empty background regions above and below the spectrum. We used boxes 35 pixels wide in the cross-dispersion direction to extract the source photons. Care was taken to exclude the area of the detector shadowed by the repeller wire when selecting the background regions. In a second step, two new event tables were created for each wavelength band from all the photon arrival times included in the previously defined source and background (x, y) region(s), respectively. Finally, these two event tables were

[3]which is strong in the raw data, but successfully subtracted in the calibrated spectrum produced by the STSDAS calibration pipeline

sampled in equally spaced time bins, i.e. light curves, and the background light curves were subtracted from the source light curves, scaled appropriately for the detector areas used in the extraction process. The light curves were converted from cts s^{-1} to fluxes by scaling to the average flux in the selected wavelength band. Figure 8 shows the background subtracted phase-folded light curves in the wavelength bands a–d, sampled in 120 s.

In order to derive amplitudes and phases of the modulations we fitted simple sine functions of the form $A \sin[(\phi - \phi_0)2\pi] + O$ to the FUV light curves, with A the half-amplitude of the sine wave, ϕ_0 the phase offset, and O the mean flux. The best-fit parameters are reported in Table 2.

At first glance, the sinusoidal FUV modulation in AR UMa is reminiscent of the FUV light curves observed in a number of polars during both high and low states and interpreted by rather large "warm" spots near the accretion regions on the white dwarfs (**?**, e.g.)]demartinoetal98-1,gaensickeetal98-2,stockmanetal94-1. In AR UMa, the phases of maximum flux ($\phi_{\max} = \phi_0 + 0.25$) vary between 0.95–1.06, which is only slightly later than the phase of maximum EUV flux during the high state. **?**) convincingly argued that the EUV flux maximum is due to the appearance of the main accreting (southern) pole during the phase interval $\sim 0.7 - 0.1$.

It seems, hence, very tempting to attribute the observed FUV modulation to a hot spot near the southern accretion region, which is either deeply heated from the previous high state (**?**, the cooling time scale of the accretion regions is ∼months,)]schmidtetal96-1 or heated by ongoing low level accretion (Sect. 3.3.3). However, two points argue against this interpretation:

(1) a spot near the southern magnetic pole would be eclipsed by the body of the white dwarf for a large part of the orbital phase, resulting in a flat-bottomed light curve (similar to the EUVE light curve, **?**), which contrasts with the observed sinusoidal shape of the FUV modulation. To match the observed shape of the FUV light curve, a southern spot would have to be ridiculously large, covering $\sim 70 - 90\%$ of the white dwarf, in which case it would be more appropriate to speak of a *cold* northern polar cap. Thus, if due to a temperature variation over the white dwarf surface, the observed FUV modulation would have to be ascribed to a hot polar cap on the northern pole. But a northern pole cap cannot reproduce the observed modulation, as its aspect changes only little with the orbital phase.

(2) the amplitude of the flux modulation is apparently not a simple function of wavelength, but shows a minimum in the 1323.2–1520.3 Å band (Table 2). This is in strong contrast to the FUV modulation observed in other polars, where the amplitude of the FUV modulation has always been found to monotonically increase toward shorter wavelengths.

To investigate the wavelength dependence of the FUV modulation in AR UMa, we extracted from the time-tagged photon lists a total of 18 phase-folded light each one covering ~ 30 Å. The signal-to-noise ratio of these light curves is of course lower than that of the four broad-band light curves, and we computed the relative modulation of a given light curve as the ratio of the standard deviation of count rate to the mean count rate in the corresponding wavelength band (Fig. 9).

As already suggested by the broad-band light curves described above, a strong modulation is observed only for $\lambda < 1300$ Å and $\lambda > 1600$ Å. The maximum modulation ($\sim 10\%$) coincides with the π component of Lyα, the minimum with the "1415 Å" absorption feature. Thus, cyclotron emission from the northern pole may dilute the modulation somewhat (Sect. 3.3.3). However, the cyclotron flux predicted from our model alone is too low to explain the observed decrease of the FUV modulation by a factor ~ 4.

Summing up, the interpretation of the FUV modulation observed with *STIS* cannot follow in a straightforward way the results obtained for other polars. Even though a hot spot may be present in AR UMa, and may contribute to the observed flux modulation, it appears likely that different phenomena cause the observed modulation at the blue and the red ends of the *STIS* bandpass. At short wavelengths the strong modulation coincides with the Lyα Zeeman absorption structure which sensitively depends on the field dependent photospheric opacities. A slight orbital variation of the projected magnetic field may thus result in a variation of the flux in this band. At long wavelengths, the broad emission bump which appears at $\phi = 0.9 - 1.1$ and which we interpreted as cyclotron emission best explains the observed flux modulation.

6.2. Probing for blobby accretion

In Sect. 3.3.3 we suggested that the bumps observed in the FUV spectrum of AR UMa are due to cyclotron emission, implying that the white dwarf is accreting at a tiny rate even during the low state. We used the *STIS* time-tagged photon stream to probe for evidence of "blobby accretion", i.e. for stochastic variability in excess to pure Poisson noise. For this analysis, we extracted a count rate light curve from the *STIS* photon stream in an analogous fashion as described above, using the entire G140L wavelength range except for a narrow range around the geocoronal Lyα emission. The background subtracted light curve, sampled in 10s bins, shows a sinusoidal modulation with an half-amplitude of 3.6 %. We computed the discrete power spectrum of this light curve using the MIDAS Time Series Analysis context (Fig. 10). Clearly present is the orbital period plus a number of aliases caused by the uneven sampling of the orbital flux modulation. In order to probe for additional non-Poissonian

power, we composed synthetic time-tagged data sets with the same mean count rate and the same coverage as the STIS data. The synthetic count rates were modulated by a sine wave with the parameters derived from the best sine-fit to the STIS count rate light curve. The synthetic data sets were sampled in 10s bins and, finally, we computed discrete power spectra from the synthetic count rate light curves. The power spectra for the synthetic data sets reproduce very well the power spectrum obtained from the real data, both the various spikes corresponding to aliases of the orbital period and the noise level at the high frequency end frequencies (Fig. 10). From this comparison, we conclude that the ultraviolet data provide no significant evidence for short-term fluctuations of the count rate due to individual accretion events down to a count rate of $\sim 0.4\,\mathrm{cts\ s^{-1}}$, corresponding to 0.1 % of the mean count rate.

7. Summary

Our analysis of the *HST/STIS* observations of AR UMa lead to the following results in our understanding of this unique accretion physics and plasma laboratory.

1. We clearly confirm the earlier *IUE* detection of the photospheric Lyα σ^+ absorption, and with an implied magnetic field strength of $\sim 200\,\mathrm{MG}$ AR UMa may well be called "the king of the polars". Alas, our state-of-the-art magnetic white dwarf model spectra fail to provide a satisfactory description of either the detailed Lyα Zeeman profiles or the ultraviolet/optical spectral energy distribution, resulting in only a rough temperature estimate, $T_{\mathrm{wd}} = 20\,000 \pm 5000\,\mathrm{K}$.

2. The uncooperative (pole-on) viewing geometry prevents a detailed mapping of either the magnetic field topology or a potential temperature variation over the white dwarf surface. Additional information can probably be obtained from the phase-dependency of the "forbidden" hydrogen $1s_0 \rightarrow 2s_0$ transition. However, detailed modeling must await the necessary atomic data.

3. As a consequence of the high field strength, the fundamental cyclotron frequency falls in the optical wavelength band. However, there is some evidence in the ultraviolet for low-harmonic cyclotron emission originating from near the magnetic pole and corresponding to a low-state accretion rate of $10^{-13}\,M_\odot\,\mathrm{yr}^{-1}$. Remnant activity in the system during the low state is also indicated by the presence of Lyα emission. The observed orbital variation of flux and velocity leads us to attribute this emission to the secondary star, possibly to a wind emanating from its trailing hemisphere.

4. The brightness and extremely low interstellar column mark AR UMa as the best polar for future FUV/EUV observations.

Support was provided through NASA grant GO-7397 from the Space Telescope Science Institute, which is operated by the Association of Universities for Research in Astronomy, Inc., under NASA contract NAS 5-26555, by the DLR grants 50 OR 99 036 and DLR 50 OR 96 173, and by the DFG grant KO 738/7-1. We thank Andreas Fischer for providing us the cyclotron emission model.

FIGURES

Fig. 1.— Right: The average G140L FUV spectrum of AR UMa and the short G230L NUV exposure (see Table 1). The mismatch between the FUV and the NUV spectra is most likely due to the different orbital phase sampling. Left: Blow-up of the Lyα region. Probable interstellar absorption lines are indicated below the spectrum, absorption and emission features intrinsic to AR UMa are indicated above the spectrum. The shaded region at the bottom gives a measure of the flux error.

Fig. 2.— Phase-resolved G140L spectra of AR UMa, orbital phases are indicated. Note the orbital variation of the $1s_0 \rightarrow 2s_0$ absorption near ~ 1180 Å and of the Lyα emission, as well as the appearance of a broad (~ 200 Å) emission bump at ~ 1650 Å during $\phi = 0.9 - 1.1$.

Fig. 3.— Combined ultraviolet/optical low state spectrum of AR UMa. The red end of the optical spectrum is dominated by the emission of the M6 secondary star. Left: illustrative comparison of the AR UMa data to non-magnetic pure hydrogen white dwarf model spectra with $T_{\rm wd} = 50\,000$ K and $T_{\rm wd} = 15\,000$ K. Both models were normalized to $V = 16.9$, the (assumed) white dwarf magnitude of AR UMa obtained by subtracting an appropriately scaled M6 spectrum from the observed low state spectrum. Right: illustrative comparison of the AR UMa data with $T_{\rm wd} = 25\,000, 20\,000, 15\,000$ K (top to bottom) magnetic white dwarf model spectra ($B = 200$ MG), again normalized to $V = 16.9$.

Fig. 4.— Dashed line: magnetic white dwarf model spectrum with $T_{\rm wd} = 17\,000$ K, $B = 200$ MG and $R_{\rm wd} = 8.2 \times 10^8$ cm (at $d = 88$ pc). Full line: *STIS* FUV data of AR UMa at $\phi = 0.5$ with the 1445 Å cyclotron component (Sect. 3.3.3) subtracted. The $1s_0 \rightarrow 2s_0$ transition is discussed in detail in Sect. 3.2.

Fig. 5.— Cyclotron emission in AR UMa. Left panel: FUV spectrum for $\phi = 0.5$ (topmost curve) and the cyclotron model derived from the 1445 Å emission bump (bottom curve). The difference of the observed FUV spectrum and the cyclotron model is shifted downwards by 0.5 units. The only available NUV spectrum is also shown, but does not match in phase ($\phi = 0.08$). Right panel: At $\phi \sim 0.0$ the FUV spectrum contains an additional emission bump

centered at ~ 1650 Å, which we attribute to cyclotron emission from the southern accretion region. Plotted are the observed FUV/NUV spectra centered on/near $\phi \sim 0.0$ (topmost curves), the cyclotron model for the 1650 Å bump (bottom curve), and the difference of the FUV ($\phi \sim 0.0$) spectrum and *both* cyclotron models (shifted downwards by 0.5 units).

Fig. 6.— Variable Lyα absorption/emission. Top panel: the observed FUV spectrum at $\phi = 0.9$ (solid line) and a damping profile corresponding to an interstellar column density $N_{\rm H} = 1.1 \times 10^{18}{\rm cm}^{-2}$. Bottom: enlargement of the phase-resolved spectra around Lyα, corrected for the interstellar absorption as displayed above. The individual spectra (from bottom to top) have been shifted upwards by 0, 3, 14, 21, and 23 units.

Fig. 7.— Velocity (top) and flux (bottom) of the Lyα emission line. The top panel shows also the best-fit sine curve to the velocity variation.

Fig. 8.— FUV light curves extracted from the time-tagged *STIS* photon stream in four wavelength bands. From top to bottom: 1146.5–1206.3 Å, 1223.9–1296.9 Å, 1323.2–1520.3 Å, 1529.1–1717.5 Å. Shown as solid lines are sine fits to the data with the parameters listed in Table 2.

Fig. 9.— Top: relative modulation of the FUV emission of AR UMa in ~ 30 Å bands. Bottom: mean FUV spectrum of AR UMa.

Fig. 10.— Power spectra of the G140L data of AR UMa (top curve) and of a simulated sine wave with a mean count rate, amplitude, period, and coverage as defined by the STIS data (bottom curve, shifted down by 4 units).

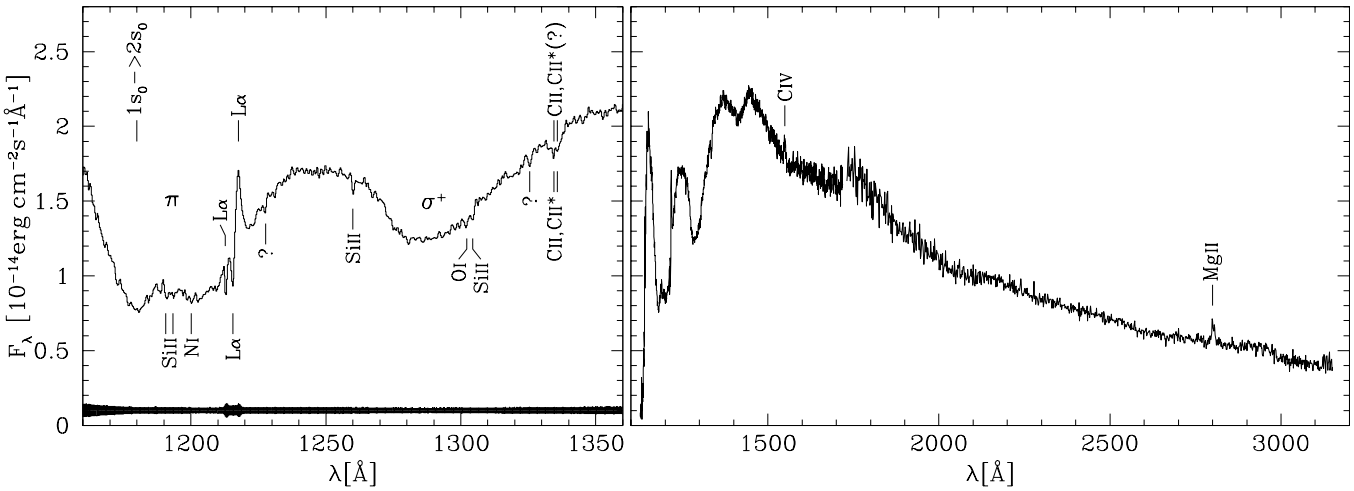

Figure 1

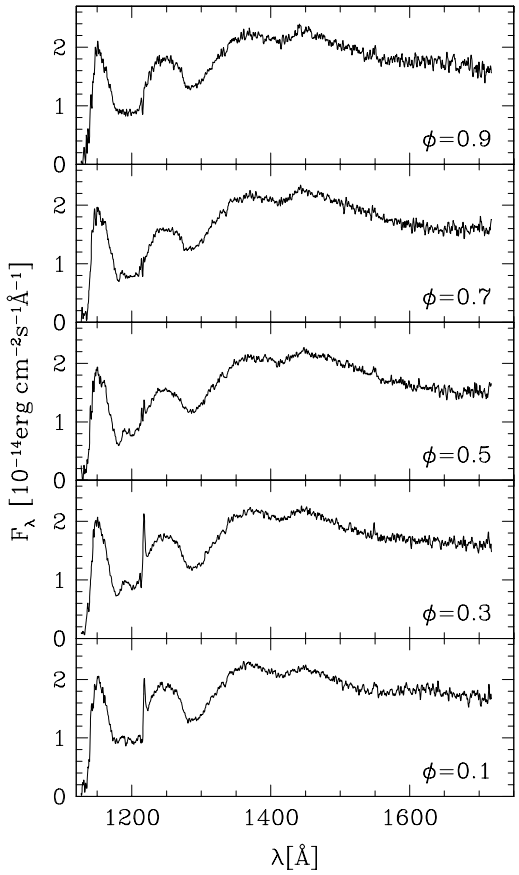

Figure 2

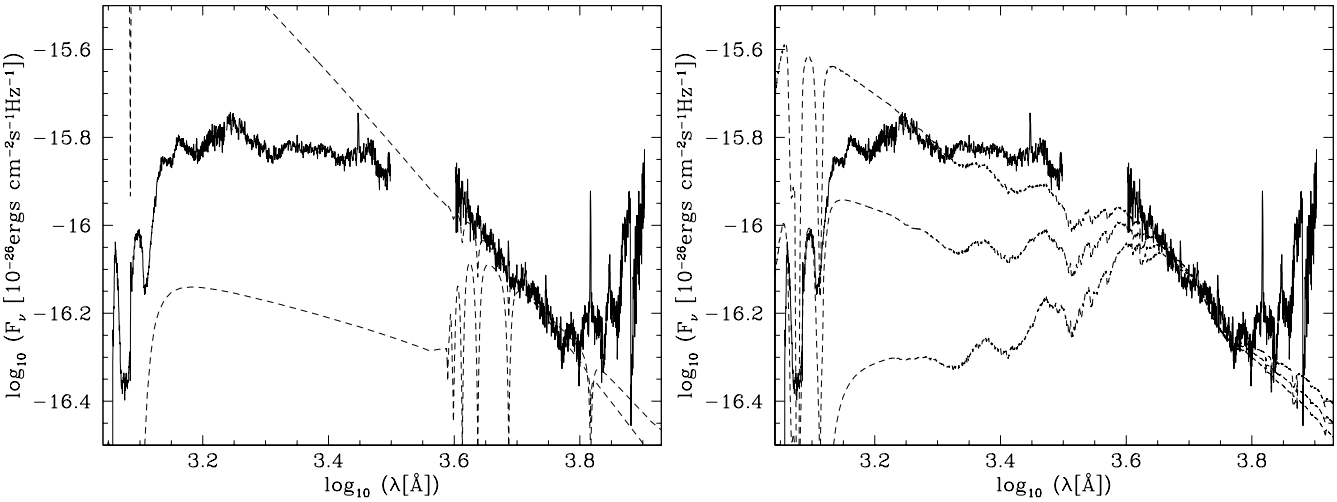

Figure 3

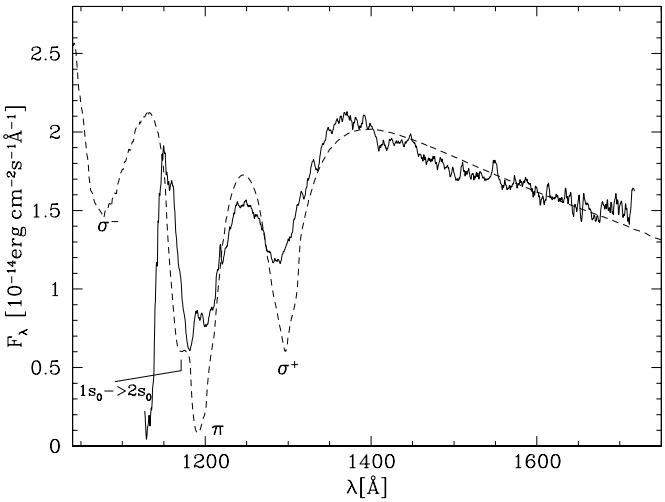

Figure 4

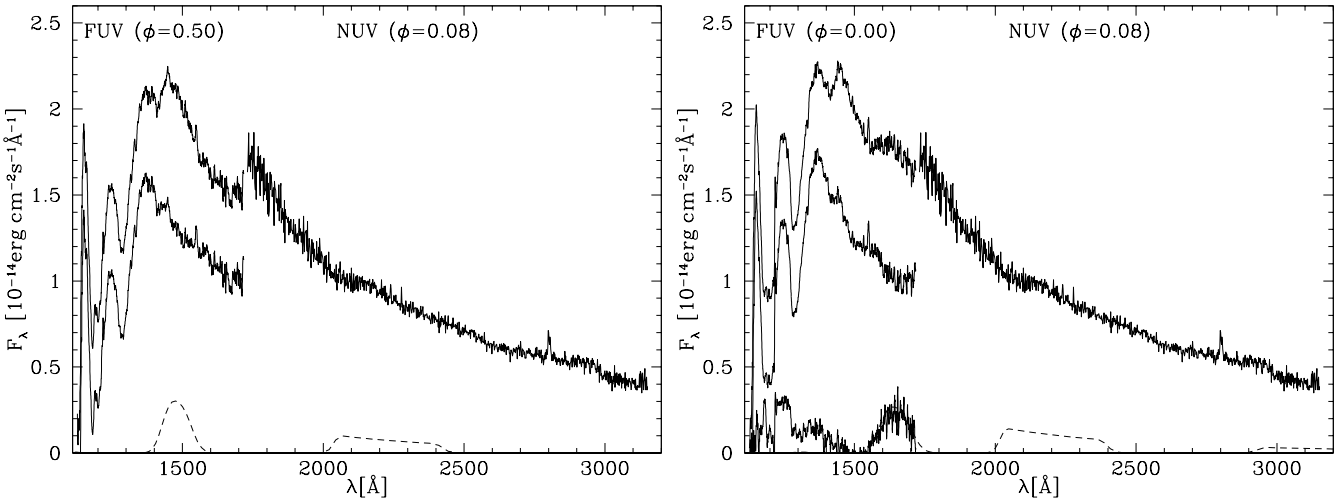

Figure 5

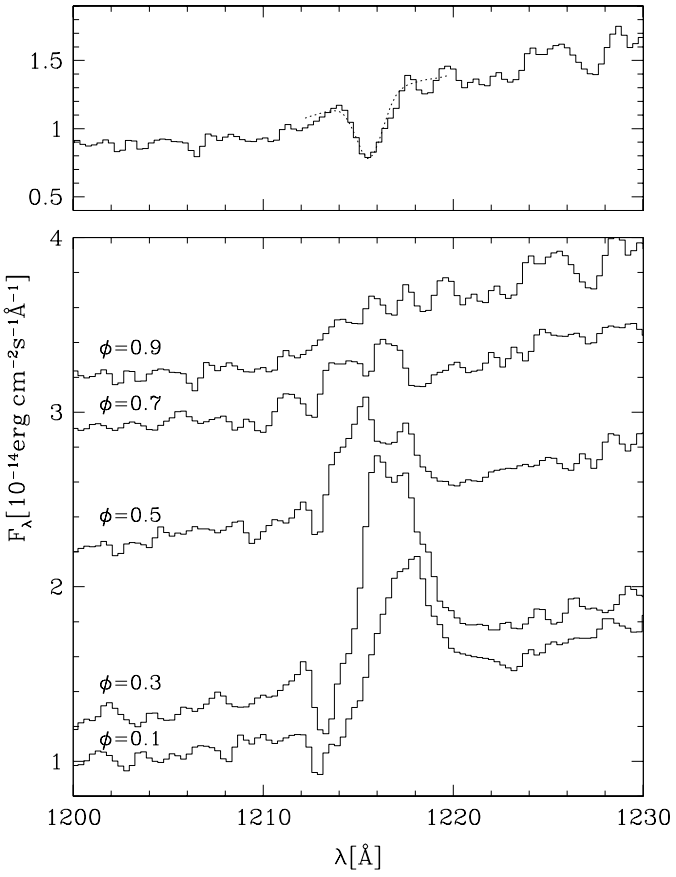

Figure 6

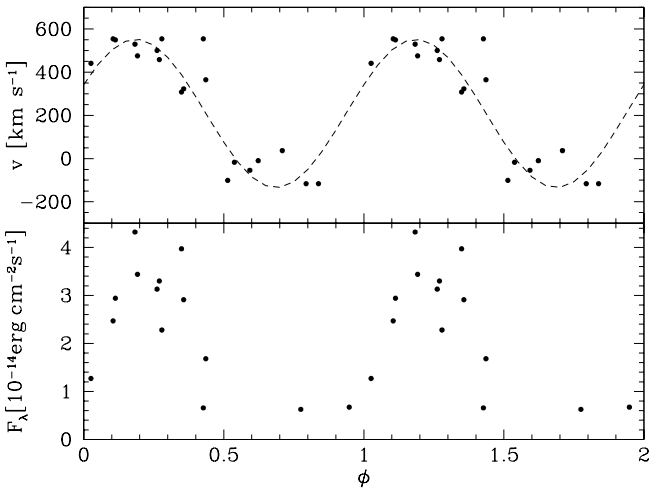

Figure 7

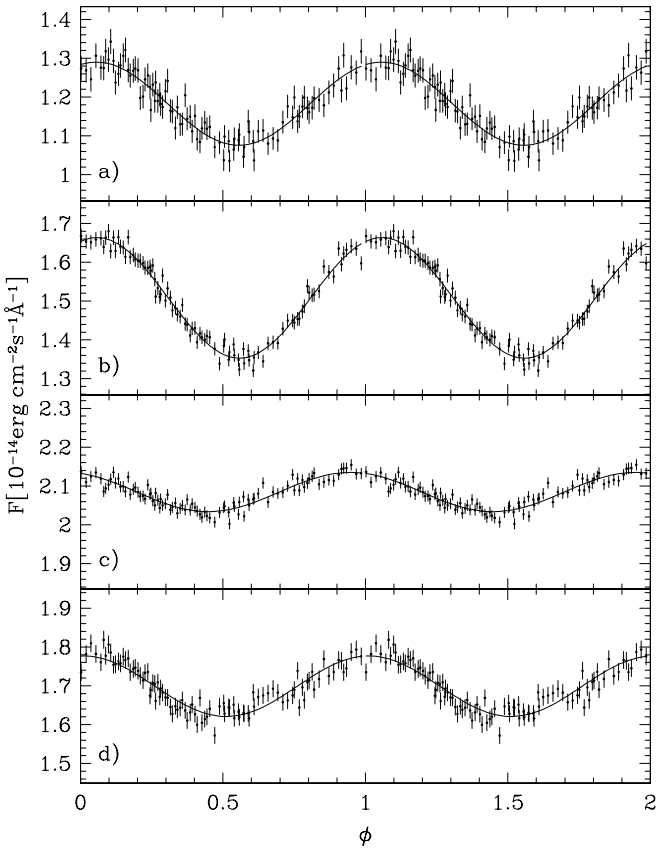

Figure 8

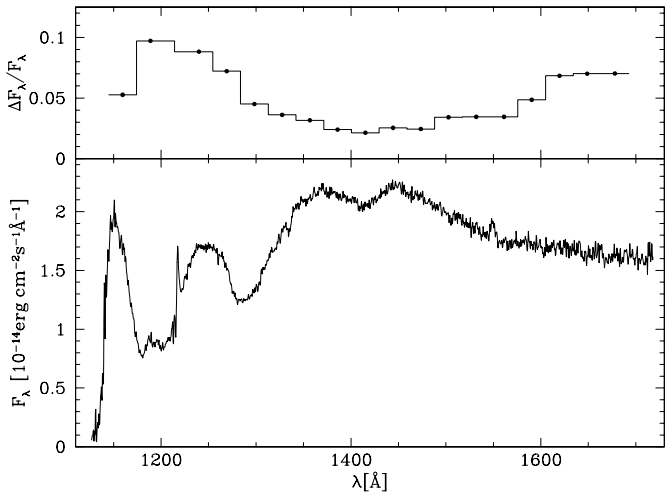

Figure 9

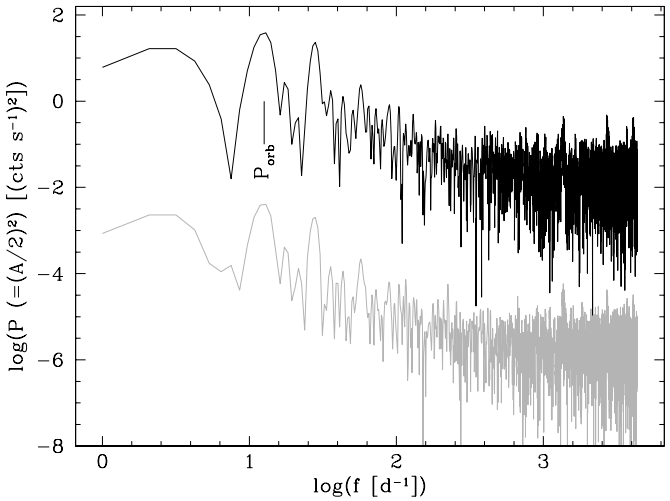

Figure 10

Table 1. Log of the *HST* observations on 1998 December 9

Dataset	Grating	Obs. start (UT)	Exp. time sec	$\Delta\phi$
o53y01010	G140L	13:26:41	2370	0.499 – 0.826
o53y01020	G140L	14:52:54	2730	0.242 – 0.622
o53y01030	G140L	16:29:39	2730	0.077 – 0.457
o53y01040	G140L	18:06:25	2730	0.912 – 0.291
o53y01050	G140L	19:43:11	1320	0.747 – 0.928
o53y01060	G230L	20:13:24	1200	0.987 – 0.159

Table 2. Wavelength bands of the ultraviolet light curves and best-fit sine parameters.

Band	λ [Å]	A	O $[10^{-14}\mathrm{erg\,cm^{-2}s^{-1}Å^{-1}}]$	$\phi_{\max}$
a	1146.5 - 1206.3	0.107	1.183	0.806
b	1223.9 - 1296.9	0.155	1.508	0.808
c	1323.2 - 1520.3	0.050	2.085	0.698
d	1529.1 - 1717.5	0.078	1.699	0.761